Multichannel-resolved dynamics in resonance-enhanced below-threshold harmonic generation of H_2^+ molecular ions

Peng-Cheng Li,[1,2] Zhi-Bin Wang,[1,3] and Shih-I Chu[4,5]

[1]*Research Center for Advanced Optics and Photoelectronics, Department of Physics, College of Science, Shantou University, Shantou, Guangdong 515063, China*

[2]*Key Laboratory of Intelligent Manufacturing Technology of MOE, Shantou University, Shantou, Guangdong 515063, China*

[3]*College of Physics and Electronic Engineering, Northwest Normal University, Lanzhou 730070, China*

[4]*Center for Quantum Science and Engineering, Department of Physics, National Taiwan University, Taipei 10617, Taiwan*

[5]*Department of Chemistry, University of Kansas, Lawrence, Kansas 66045, USA*

(Received 15 December 2020; revised 12 March 2021; accepted 30 March 2021; published 16 April 2021)

Recently the study of the resonance-enhanced below-threshold harmonic generation (BTHG) of atoms and molecules has received considerable attention. BTHG, with spatially coherent and high conversion efficiency, can provide a potential way to produce powerful vacuum-ultraviolet light sources. However, the resonance effects associated with molecular BTHG have become more complex to study due to the presence of the extra internuclear degree of freedom. Here we perform an *ab initio* study and demonstrate the multichannel-resolved dynamics in resonance-enhanced BTHG of H_2^+ molecular ions by combining a synchrosqueezing time-frequency transform with an extended semiclassical simulation. We find that BTHG of H_2^+ on resonance is enabled only near the zero-laser field region and the multichannel interference is responsible for enhanced BTHG. The time-frequency spectra in the vicinity of the resonance exhibit a periodic split structure with oscillating laser pulses and can be explained by the individual dynamical behavior of multiple channels in BTHG.

DOI: 10.1103/PhysRevA.103.043113

I. INTRODUCTION

High-order harmonic generation (HHG) from atoms and molecules is a fundamental strong-field process that attracts substantial attention in ultrafast science and technology [1], since it provides a potential way to predict the source of very bright, short-pulse, high-frequency coherent radiation. Laser pulses as short as an attosecond timescale can probe the electronic dynamics in atomic and molecular systems [2–5]. The HHG spectrum exhibits a rapid drop at the first few harmonics followed by a broad plateau where all the harmonics have a similar amplitude and then a cutoff with the dramatic decrease of harmonic intensity. The semiclassical recollision model developed by Corkum [6] and Kulander [7] demonstrated that the maximum kinetic energy of a classical electron rescattering with the atomic core is $3.17U_p$, where U_p is the ponderomotive energy. Thus the highest energy of the harmonic emission is $I_p+3.17U_p$, where I_p is the atomic ionization potential.

Molecules subject to intense laser fields introduce new dynamical behaviors in HHG due to the extra degrees of freedom of internuclear distance. Even the simplest molecules show considerably more complicated responses to strong fields than that of atoms and pose additional challenge to researchers. Thus the study of HHG from small diatomic molecules in intense laser pulses continues to receive considerable current interest both theoretically and experimentally [8]. Most previous studies of molecular HHG have focused on the study of the sensitivity of the HHG efficiency on the orientation of the molecular axis with respect to the polarization of the laser field and related two-center interference phenomena [9–16]. Recently, the below-threshold harmonic generation (BTHG) from atoms and molecules [17–24] in the intense laser fields has become a subject of immense interest due to high conversion efficiency for producing the vacuum-ultraviolet strong light sources. For example, Chini *et al.* [25] have shown that the phase-matched below-threshold harmonics are generated only near the resonance structures of the atomic target. Soifer *et al.* [26] have studied the near-threshold harmonic generation with aligned molecules. However, the resonant effects in both atoms and molecules in the intense laser fields are still an open problem; in particular it is more of a challenge to explain the features present in resonance-enhanced molecular BTHG than that of atoms.

In this work, we present an *ab initio* quantum study of BTHG from H_2^+ molecular ions in the presence of an intense laser field by solving the three-dimensional time-dependent Schrödinger equation (TDSE) accurately and efficiently by means of the time-dependent generalized pseudospectral method in prolate spheroidal coordinates [27,28]. Combining with a synchrosqueezed transform (SST) technique [29–31] and an extended semiclassical analysis, we evaluate the contribution of each nucleus to the BTHG of H_2^+ molecular ions. This allows us to identify multiple-channel contributions, which are relevant to the electron driven initially at the specific time of the laser pulse from one nuclear core to either the neighboring ion or the parent ion itself. We find that the multichannel interference responsible for resonance-enhanced

BTHG of H_2^+ occurs only near the zero-laser field. Furthermore, we work out an intuitive physical picture for revealing the detailed electron dynamics in BTHG of H_2^+.

II. THEORETICAL METHOD

HHG is produced by the interaction of an intense laser field with the hydrogen molecular ion H_2^+, which can be studied by solving the following TDSE (in atomic units):

$$i\frac{\partial}{\partial t}\Psi(\mathbf{r},t) = [H_0 + V_{ext}(\mathbf{r},t)]\Psi(\mathbf{r},t). \tag{1}$$

Here $V_{ext}(\mathbf{r},t)$ is the time-dependent molecule-field interaction and H_0 represents the unperturbed molecule Hamiltonian, which can be written as

$$H_0 = -\tfrac{1}{2}\nabla^2 + U(\mathbf{r}), \tag{2}$$

where $-\frac{1}{2}\nabla^2$ is the kinetic energy operator and $U(\mathbf{r})$ is the Coulomb interaction with the nuclei.

To describe the diatomic molecular ion H_2^+, we make use of the prolate spheroidal coordinates ξ, η, and φ, which are related to the Cartesian coordinates x, y, and z as follows:

$$\begin{aligned} x &= a\sqrt{(\xi^2-1)(1-\eta^2)}\cos\varphi, \\ y &= a\sqrt{(\xi^2-1)(1-\eta^2)}\sin\varphi, \\ z &= a\xi\eta \quad (1 \leqslant \xi < \infty, -1 \leqslant \eta \leqslant 1). \end{aligned} \tag{3}$$

In Eq. (3) we assume that the molecular axis is directed along z axis, and the nuclei are located on this axis at the positions $-a$ and a, so the internuclear separation $R = 2a$. In the linearly polarized and the dipole approximation, we can also assume that the polarization vector of the field lies in the plane x-z. Then using the length gauge and the prolate spheroidal coordinates, the time-dependent molecule-field interaction $V_{ext}(\mathbf{r},t)$ can be written as follows:

$$\begin{aligned} &V_{ext}(\xi,\eta,\varphi,t) \\ &\quad = aE(t)[\xi\eta\cos\beta + \sqrt{(\xi^2-1)(1-\eta^2)}\cos\varphi\sin\beta]. \end{aligned} \tag{4}$$

Here β is the angle between the polarization vector of the laser field and the molecular axis, and $E(t)$ is the time-dependent laser field. The unperturbed molecule Hamiltonian H_0 in the prolate spheroidal coordinates is given by

$$H_0 = -\tfrac{1}{2}\nabla^2 + U(\xi,\eta). \tag{5}$$

Here the kinetic energy operator in the prolate spheroidal coordinates has the following form:

$$\begin{aligned} -\frac{1}{2}\nabla^2 = -\frac{1}{2a^2}\frac{1}{(\xi^2-\eta^2)}\Bigg[&\frac{\partial}{\partial\xi}(\xi^2-1)\frac{\partial}{\partial\xi} + \frac{\partial}{\partial\eta}(1-\eta^2)\frac{\partial}{\partial\eta} \\ &+ \frac{\xi^2-\eta^2}{(\xi^2-1)(1-\eta^2)}\frac{\partial^2}{\partial\varphi^2}\Bigg], \end{aligned} \tag{6}$$

and the Coulomb interaction with the nuclei is given by (the charge of each center is unity)

$$U(\xi,\eta) = -\frac{2\xi}{a(\xi^2-\eta^2)}. \tag{7}$$

To calculate the HHG spectra, we solve the TDSE for the molecule H_2^+ in the laser field. The initial wave function is an unperturbed eigenfunction of H_2^+. We obtain the eigenvalues and eigenfunctions by means of the generalized pseudospectral method [27]. Detailed numerical procedures can be found in Refs. [32] and [33]. We propagate the time-dependent wave function using the second-order split-operator method in the energy representation:

$$\begin{aligned} \Psi(t+\Delta t) = &\exp\left(-i\frac{1}{2}\Delta t H_0\right) \\ &\times \exp\left[-i\Delta t V(\xi,\eta,t+\frac{1}{2}\Delta t)\right] \\ &\times \exp\left(-i\frac{1}{2}\Delta t H_0\right)\Psi(t) + O((\Delta t)^3). \end{aligned} \tag{8}$$

Once the time-dependent wave function is available, we can proceed to calculate the spectra of the emitted harmonic radiation. In order to calculate the HHG spectra, we employ the general semiclassical approach by substituting the classical quantities with the corresponding quantum expectation values. The spectral density of the harmonic radiation energy is given by either the length form

$$S(\omega) = \frac{2\omega^4}{3\pi c^3}|\mathbf{D}_\omega|^2 \tag{9}$$

or the acceleration form

$$S(\omega) = \frac{2}{3\pi c^3}|\mathbf{A}_\omega|^2. \tag{10}$$

Here $\mathbf{D}_\omega$ and $\mathbf{A}_\omega$ are the Fourier transforms of the time-dependent dipole moment $D(t)$ and dipole acceleration $A(t)$, respectively. The length and acceleration forms provide almost identical results for the HHG spectra, indicating good quality of our calculated wave functions.

The dynamics of the HHG process can be explored in more detail using the time-frequency analysis of the dipole acceleration by means of the synchrosqueezed transformation (SST) [29–31]. The SST is defined by

$$S(t,\xi) = \int V(t,\omega)\frac{1}{\alpha}h\left(\frac{|\xi-\omega_f(t,\omega)|}{\alpha}\right)d\omega, \tag{11}$$

where $\alpha > 0$, $h(t) = e^{-t^2}/\sqrt{\pi}$. $V(t,\omega)$ is the modified wavelet transform of the harmonic spectra, which can be written as

$$V(t,\omega) = \int A(t')\sqrt{\omega}W[\omega(t'-t)]\,dt', \tag{12}$$

where the Morlet wavelet $W(x)$ is defined as

$$W(x) = \frac{1}{\sqrt{\tau}}e^{ix}e^{\frac{-x^2}{2\tau^2}}. \tag{13}$$

The instantaneous frequency information function $\omega_f(t,\omega)$ is defined by

$$\omega_f(t,\omega) = \begin{cases} \dfrac{-i\partial_t V(t,\omega)}{V(t,\omega)}, & \text{for} \quad V(t,\omega) \neq 0 \\ \infty, & \text{for} \quad V(t,\omega) = 0 \end{cases}. \tag{14}$$

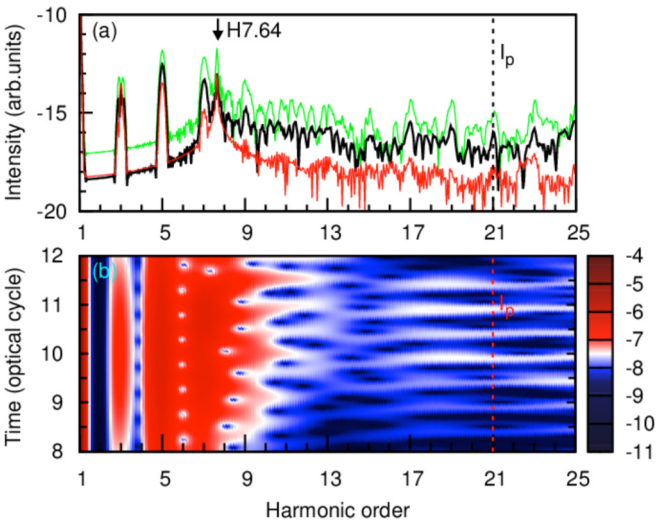

FIG. 1. (a) Below-threshold harmonic generation of H_2^+ driven by an 800-nm laser pulse with a peak intensity of $I = 1.0 \times 10^{14}$ W/cm^2 (red solid lines), $I = 1.5 \times 10^{14}$ W/cm^2 (black solid lines), and $I = 2.0 \times 10^{14}$ W/cm^2 (green solid lines), respectively. The black vertical dashed line indicates the ionization threshold of the $1\sigma_g$ state marked by I_p at $R = 2$ a.u., and the black arrow indicates that the resonant structure is located at the harmonic 7.64 (H7.64), which corresponds to the bound-bound transition from $1\sigma_g$-$1\sigma_u$. (b) Wavelet time-frequency spectra of BTHG for the case of the peak intensity $I = 2.0 \times 10^{14}$ W/cm^2 in (a).

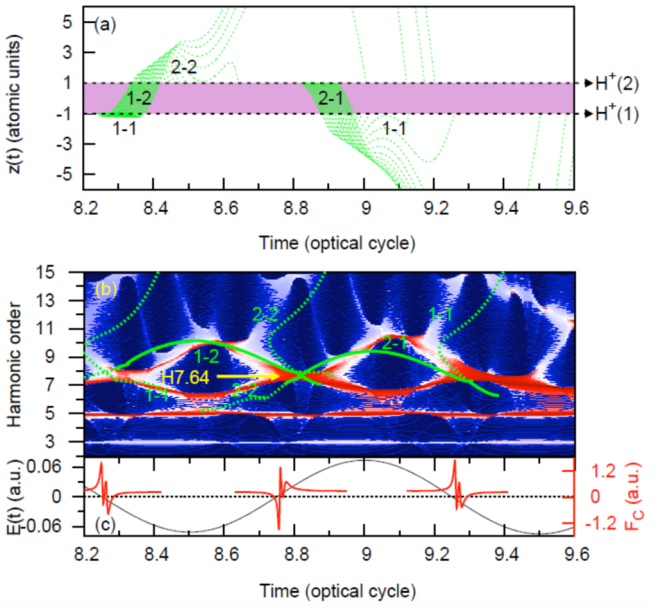

FIG. 2. (a) The electronic trajectories as a function of the emission time. (b) SST time-frequency spectra of BTHG of H_2^+ for the case of the peak intensity $I = 2.0 \times 10^{14}$ W/cm^2 as shown in Fig. 1(a). The yellow arrow indicates that the harmonic generation on resonant (H7.64). For reference, the green curves indicate semiclassical return energy as a function of the emission time. Note that the multiple channels which relate to the electron driven initially by the lasers field at specific time of the laser pulse from one nuclear core to either the neighboring ion or parent ion itself are marked by the quantum paths 1-1, 1-2, 2-2, and 2-1, respectively. (c) The laser field $E(t)$ and Coulomb-field force F_C as a function of the time. The other laser parameters used are the same as those in Fig. 1.

In our calculation, the time-frequency characteristics of the HHG are analyzed by means of the SST based on wavelet transform of the time-dependent dipole acceleration.

III. RESULTS AND DISCUSSIONS

In Fig. 1(a) we present BTHG of H_2^+ molecular ions in an 800-nm laser field with a peak intensity of $I = 1.0 \times 10^{14}$ W/cm^2, $I = 1.5 \times 10^{14}$ W/cm^2, and $I = 2.0 \times 10^{14}$ W/cm^2. In our calculation, the laser field is written as $E(t) = E_0 \cos^2(\pi t/NT)\cos(\omega t)$. Here E_0 is the electric field amplitude, ω is the frequency, and T is the duration of one optical cycle. The total duration is equal to $N = 20$ optical cycles. The black vertical dashed lines indicate the ionization threshold of the initial state marked by I_p, where I_p is equal to -1.103 a.u. for the $1\sigma_g$ state at the equilibrium internuclear separation of $R = 2$ a.u., which coincides with the 19.4th harmonic order for the 800-nm laser wavelength. Considering the shift of the threshold energy in the laser field, we assume that the ionization threshold is located at the 21st harmonic. The ionization energy of σ_u state is -0.668 a.u. at $R = 2$ a.u., and the black arrow indicates that the resonant peak is located at the 7.64th harmonic (H7.64) which corresponds to the bound-bound transition from $1\sigma_g$-$1\sigma_u$. As the driving laser intensity is further increased to $I = 2.0 \times 10^{14}$ W/cm^2, the resonant peaks almost overlap, but it is still located at H7.64. After increasing the driving laser intensity to $I = 3.0 \times 10^{14}$ W/cm^2, the peaks become broadened (not shown here). The reason is that the yield of the resonant harmonic H7.64 is sensitive to the laser intensity. In Fig. 1(b) we present the wavelet transform of time-frequency spectra of BTHG of H_2^+ for the case shown in Fig. 1(a) for the peak intensity of $I = 2.0 \times 10^{14}$ W/cm^2. It is clearly seen that the wavelet time-frequency spectra of H_2^+ below the ionization threshold are subject to some obscure features due to the broadband width in time-frequency distribution. Thus, the wavelet time-frequency transform has a limitation in revealing the spectral features below the ionization threshold.

To circumvent the limitation of the traditional time-frequency transform and to uncover the electronic dynamics in BTHG of H_2^+, we perform the time-frequency analysis of the dipole acceleration by means of the SST, and we find that the SST is capable of revealing the characteristic behaviors of harmonic spectra below the ionization threshold [31,34]. The advantage of the SST as compared to other widely used time-frequency transforms is its capability to generate sharper and clearer time-frequency distributions, which then allows us to identify the individual role of multiple channels below the ionization threshold in the time-frequency domain. On the other hand, a semiclassical model gives a fairly satisfied description of the laser-driven dynamical behavior of the electrons, and it has been successfully extended to extract the dynamical behaviors of the laser-driven rescattering in molecular BTHG [35].

Figure 2(a) shows several electronic paths calculated by an extended semiclassical model for the case of the peak intensity $I = 2.0 \times 10^{14}$ W/cm^2 as shown in Fig. 1(a). In our

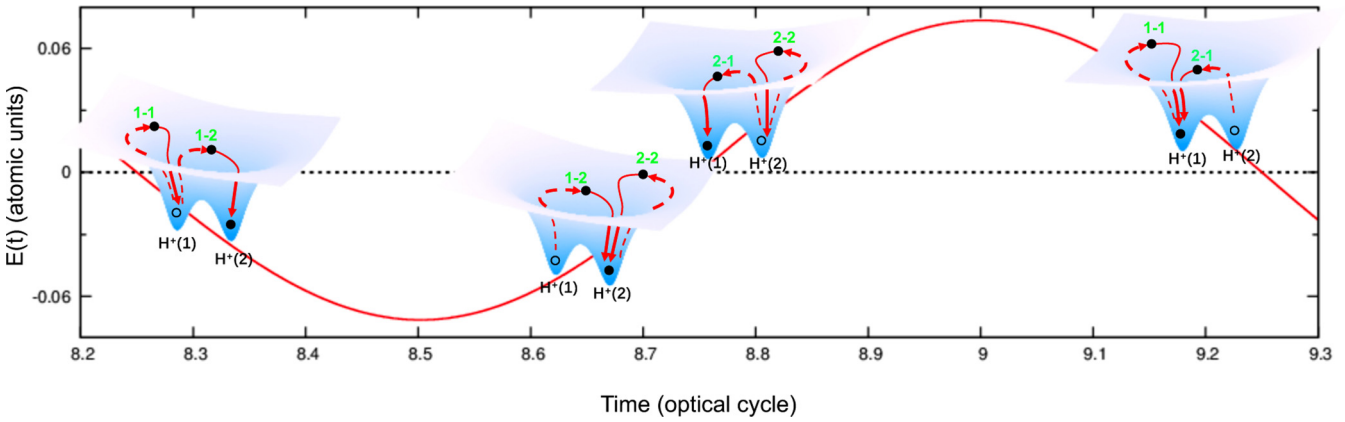

FIG. 3. Dynamical schemes of the electronic behaviors in BTHG of H_2^+ with driving laser field.

calculations, the semiclassical results are obtained by solving the three-dimension Newton's equation which takes into account the molecular potential, which is given by

$$\ddot{\mathbf{r}} = -\nabla U(\mathbf{r}) - E(t)\mathbf{e}_z, \tag{15}$$

where $U(\mathbf{r})$ is the molecular potential of H_2^+, $-\nabla U(\mathbf{r})$ is the Coulomb force F_C, and $-E(t)$ is the electric field force in the z direction. The initial condition used is electrons with an initial kinetic energy released along or against the polarized direction of laser fields at the nuclear core $H^+(1)$ or $H^+(2)$. Note that the multiple channels which relate to the electron driven initially by the lasers field at a specific time of the laser pulse from one nuclear core to either the neighboring ion or parent ion itself are marked by the quantum paths 1-1, 1-2, 2-2, and 2-1, respectively.

Figure 2(b) shows the corresponding SST time-frequency analysis of the BTHG spectra of H_2^+ calculated by the accurate treatment of the TDSE. One readily observes a clear time-frequency spectra of BTHG. The spectral and temporal characteristics of the BTHG show a periodic split of time-frequency spectra between the fifth harmonic and the 11th harmonic. For reference, the green curves indicate semiclassical return energy as a function of the emission time. Combining with the SST time-frequency spectra and an extended semiclassical return energy map, the distinct contribution of the multiple channels can be recognized. The semiclassical results are in good agreement with the SST time-frequency analysis of the BTHG spectra of H_2^+. We find that the channels 1-2, 2-2, and 2-1 overlap at 8.3 optical cycle (o.c.), 8.8 o.c., and 9.3 o.c., where the laser field is almost zero. It is interesting to note that these overlaps are just located at the resonant harmonic H7.64. It implies that the multichannel interference is responsible for resonant BTHG.

In Fig. 2(c) we show the laser field $E(t)$ and the Coulomb-field force F_C as a function of the time. The Coulomb force F_C is dominant at 8.3 o.c., 8.8 o.c., and 9.3 o.c., where the interference occurs just between the channels 1-2, 2-2, and 2-1. It indicates that the Coulomb potential plays an important role in multichannel interference. On the other hand, the individual evolution of multiple channels 1-1,1-2, 2-2, and 2-1 is responsible for the periodic split of time-frequency spectra of BTHG. Although the two nuclear cores of H_2^+ are symmetrical, the harmonic emission associated with the evolution of the channels is different. In the channels in BTHG shown in Fig. 2(b), the evolution of the electronic behaviors starts from the channels 1-1,1-2, and 2-2 in half of one optical cycle and follows from channels 2-2, 2-1, and 1-1 in another half of one optical cycle when the laser field changes sign. Obviously, the electron revisits two nuclear cores in BTHG alternately in every optical cycle. Our findings lead to a deeper understanding of multichannel-resolved dynamics in resonance-enhanced BTHG of H_2^+ molecular ions.

To better understand the dynamical behavior of the electrons in resonance-enhanced BTHG of H_2^+ molecular ions, we present below the dynamical schemes of the electronic behaviors in BTHG of H_2^+ as shown in Fig. 3. The red solid lines indicate the laser field $E(t)$. These dynamical schemes demonstrate the evolutions of the multiple channels in BTHG of H_2^+ with a driving laser field. First, in channel 1-1, the electron is released against the electric field force at the nuclear core $H^+(1)$, so the electron is driven back quickly to the parent core itself. Then, in channel 1-2, the electron is driven from the parent core $H^+(1)$ to the neighbor core $H^+(2)$. Last, in channel 2-2, the electron is driven back to the nuclear core $H^+(2)$. Note that the contributions of the channel 1-2 have two different dynamical behaviors: one happens at the rising part of each one half optical cycle, another one happens at the falling part of each one-half optical cycle where the laser intensity is always small. In fact, the contributions of the channel 2-2 also have two different dynamical behaviors: one is at the falling part of each one-half optical cycle, where the Coulomb-field force pulls the electron back to the nuclear core H_2^+ rapidly when the laser intensity is almost zero. This indicates that the Coulomb potential plays an important role in multichannel evolution. The other dynamical behavior of the channel 2-2 shows up at the rising part of each one-half optical cycle where the laser field just reverses the direction, and the amplitude is small. The three distinct channels 1-2, 2-2, and 2-1 are responsible for the resonance-enhanced BTHG of H_2^+ near the zero-laser field. Our result provides a comprehensive physical picture for the deeper understanding of the multichannel interference.

To check the sensitivity of the channels 1-2, 2-2, 2-1, and 1-1 in BTHG of H_2^+ to the laser wavelength, we show BTHG of H_2^+ molecular ions driven by the 1064-nm laser pulse with the intensity $I = 2.0 \times 10^{14}$ W/cm^2 as shown in Fig. 4(a).

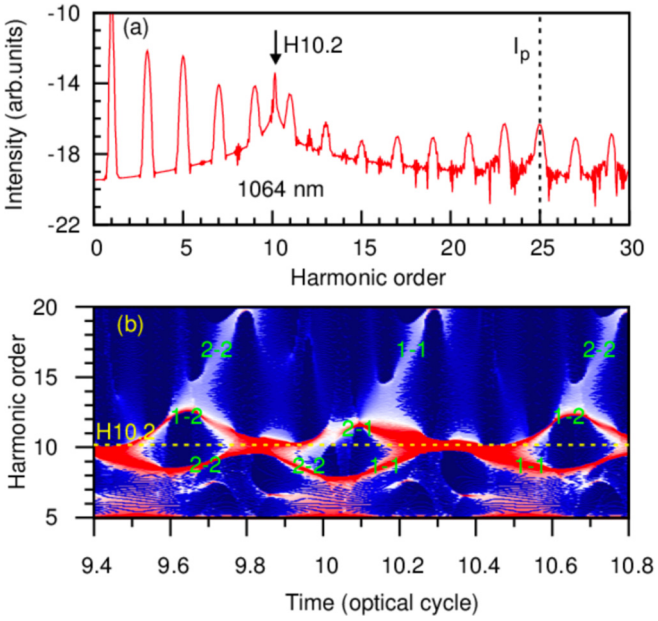

FIG. 4. (a) Below-threshold harmonic generation of H_2^+ molecular ions driven by the 1064-nm laser pulse with the intensity $I = 2.0 \times 10^{14}$ W/cm^2. The black solid arrow indicates that the resonant structure is located at the 10.2nd harmonic (H10.2). The other laser parameters used are the same as those in Fig. 1. (b) The corresponding SST time-frequency spectra. The yellow horizontal dashed line indicates the resonant structure at harmonic H10.2. The multiple channels are marked by 1-1, 1-2, 2-2, and 2-1, respectively.

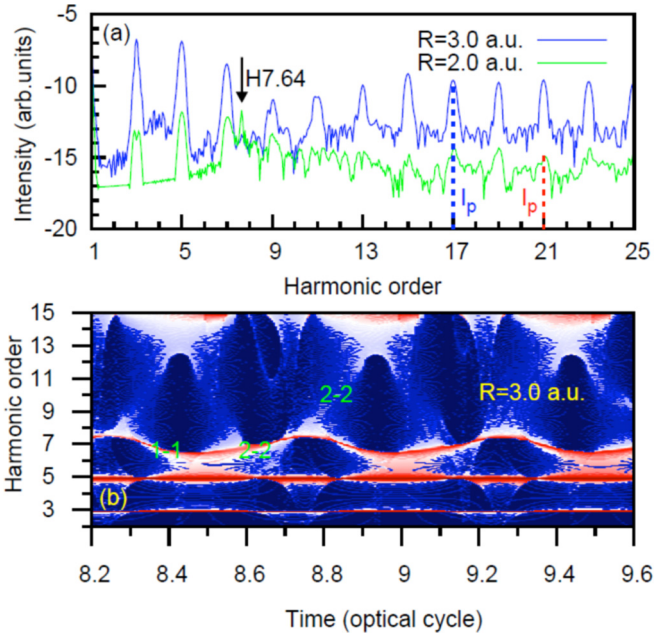

FIG. 5. (a) Below-threshold harmonic generation of H_2^+ molecular ions driven by the 800-nm laser pulse with the internuclear distance $R = 3.0$ a.u. and $R = 2.0$ a.u., respectively. The other laser parameters used are the same as those in Fig. 1. The red and blue vertical dashed lines indicate the ionization threshold marked by I_p, and the black arrow indicates that the resonant structure is located at the harmonic H7.64. (b) The SST time-frequency spectra of the BTHG for the case of the internuclear distance $R = 3.0$ a.u. in (a).

The other laser parameters used are the same as those in Fig. 1. For the 1064-nm laser pulse case, the resonant peak between the bound-bound transition from $1\sigma_g$-$1\sigma_u$ is located at the 10.2nd harmonic (H10.2). We find that the SST time-frequency spectra of the BTHG as shown in Fig. 4(b) also show a periodic split. As in the discussion above, a similar dynamical origin leads to this phenomenon. This implies that the multiple channels in BTHG of H_2^+ are not sensitive to the laser wavelength, but the yields of the harmonics are dependent on the laser-field intensity.

Finally, we check how sensitive the channels 1-2, 2-2, 2-1, and 1-1 in BTHG of H_2^+ are to the internuclear distance. In Fig. 5(a) we show a comparison of BTHG of the H_2^+ molecule at the internuclear distance $R = 3.0$ a.u. and $R = 2.0$ a.u. The other laser parameters used are the same as those in Fig. 1. For the $R = 3.0$ a.u. case, the ionization energy of the σ_g state is -0.9109 a.u. and that of the σ_u state is -0.7014 a.u. So the resonant peak between the bound-bound transition from $1\sigma_g - 1\sigma_u$ is located near the harmonic 3.7, and the resonant peak with $R = 2.0$ a.u. disappears near the harmonic H7.64. In Fig. 5 (b) we find that the SST time-frequency spectra of BTHG do not show a periodic split structure, indicating that the contribution of either the channel 2-1 or the channel 1-2 in BTHG is sensitive to the internuclear distance. This implies that the channels 1-2 and 2-1 in BTHG of H_2^+ are sensitive to the internuclear distance, because the interference of the channels 1-2 and 2-1 is decreased due to the larger internuclear distance, where the dynamics in HHG is similar to atoms when the internuclear distance is increased.

IV. CONCLUSION

In conclusion, we have presented an *ab initio* study and detailed analysis of the harmonic generation of H_2^+ below the ionization threshold in the intense laser fields by accurately solving the TDSE. We find that the distinct multiple channels contributing to the BTHG of H_2^+ are related to the electron driven by the laser field at a specific time of the laser pulse from one nuclear core to either the neighboring ion or parent ion itself. The role of multiple channels on BTHG of H_2^+ is explored by combining the SST transform of the quantum time-frequency spectrum with an extended semiclassical analysis. The results show that the multichannel interference responsible for the resonant enhanced molecular BTHG occurs only near zero-laser field, where the Coulomb potential plays the crucial role. In addition, we find that the multiple channels in BTHG of H_2^+ are not sensitive to the laser wavelength and the laser intensity, but the yields of the harmonics are dependent on the laser-field intensity. Our results and analysis enable us to obtain a deeper understanding of below-threshold molecular harmonics.

As in the discussion above, the multichannel interference is responsible for the resonant BTHG. However, the orientation effects are strongly affected by the symmetry of the wave function and the corresponding distribution of the electron density [33]. It implies that the multichannel dynamics are dependent on the symmetry properties of the molecular orbitals, which can lead to either enhancement or suppression

of the harmonic generation. In addition, the nuclear symmetry also influences the channel selection for the BTHG; our previous work [35] indicates that the asymmetric molecules play an important role in the constructive interference of multiple quantum channels, leading to a significant enhancement of the BTHG. Although our result is for the one-electron molecular case, the insights obtained are quite general and still applicable for the understanding of multichannel-resolved dynamics in resonance-enhanced BTHG for multielectron molecules, because the previous findings show that the commonly used one-electron model, namely, using only the highest-occupied molecular orbital, can be insufficient for the proper description of the HHG in multielectron molecules.

ACKNOWLEDGMENTS

This work was supported by the National Natural Science Foundation of China (Grants No. 11674268, No. 11764038, No. 91850209, and No. 12074239), Natural Science Foundation of Guangdong Province (Grants No. 2020A1515010927, No. 200110165892233, and No. 210206153460124), Department of Education of Guangdong Province (Grants No. 2018KCXTD011, No. 2019KTSCX038, and No. 2020KCXTD012), and Shantou University (Grant No. NTF18030). We also would like to acknowledge the partial support of National Taiwan University (Grants No. 110L890101 and No. 110L104048) as well as the Ministry of Science and Technology (Grant No. 109CA103), Taiwan.

[1] F. Krausz and M. Ivanov, Rev. Mod. Phys. **81**, 163 (2009).
[2] M. Chini, K. Zhao, and Z. H. Chang, Nat. Photonics **8**, 178 (2014).
[3] S. Haessler, J. Caillat, W. Boutu, C. Giovanetti-Teixeira, T. Ruchon, T. Auguste, Z. Diveki, P. Breger, A. Maquet, B. Carré *et al.*, Nat. Phys. **6**, 200 (2010).
[4] S. Baker, J. S. Robinson, C. A. Haworth, H. Teng, R. A. Smith, C. C. Chirila, M. Lein, J. W. G. Tisch, and J. P. Marangos, Science **312**, 424 (2006).
[5] J. Henkel, T. Witting, D. Fabris, M. Lein, P. L. Knight, J. W. G. Tisch, and J. P. Marangos, Phys. Rev. A **87**, 043818 (2013).
[6] P. B. Corkum, Phys. Rev. Lett. **71**, 1994 (1993).
[7] K. C. Kulander, K. J. Schafer, and J. L. Krause, in *Proc. Workshop on Super-Intense Laser Atom Physics (SILAP) III*, edited by P. Piraux (Plenum Press, New York, 1993), p. 95.
[8] J. H. Posthumus, Rep. Prog. Phys. **67**, 623 (2004).
[9] M. Yu. Ivanov and P. B. Corkum, Phys. Rev. A **48**, 580 (1993).
[10] T. Zuo, S. Chelkowski, and A. D. Bandrauk, Phys. Rev. A **48**, 3837 (1993).
[11] M. Lein, P. P. Corso, J. P. Marangos, and P. L. Knight, Phys. Rev. A **67**, 023819 (2003).
[12] R. Velotta, N. Hay, M. B. Mason, M. Castillejo, and J. P. Marangos, Phys. Rev. Lett. **87**, 183901 (2001).
[13] V. Averbukh, O. E. Alon, and N. Moiseyev, Phys. Rev. A **64**, 033411 (2001).
[14] M. F. Ciappina, C. C. Chirilă, and M. Lein, Phys. Rev. A **75**, 043405 (2007).
[15] R. Kopold, W. Becker, and M. Kleber, Phys. Rev. A **58**, 4022 (1998).
[16] A. D. Bandrauk and H. Yu, Phys. Rev. A **59**, 539 (1999).
[17] E. P. Power, A. M. March, F. Catoire, E. Sistrunk, K. Krushelnick, P. Agostini, and L. F. DiMauro, Nat. Photonics **4**, 352 (2010).
[18] D. C. Yost, T. R. Schibli, J. Ye, J. L. Tate, J. Hostetter, M. B. Gaarde, and K. J. Schafer, Nat. Phys. **5**, 815 (2009).
[19] J. A. Hostetter, J. L. Tate, K. J. Schafer, and M. B. Gaarde, Phys. Rev. A **82**, 023401 (2010).
[20] W. H. Xiong, J. W. Geng, J. Y. Tang, L. Y. Peng, and Q. H. Gong, Phys. Rev. Lett. **112**, 233001 (2014).
[21] Beaulieu *et al.*, Phys. Rev. Lett. **117**, 203001 (2016).
[22] K. N. Avanaki, D. A. Telnov, and S. I. Chu, Phys. Rev. A **90**, 033425 (2014).
[23] J. Heslar and S. I. Chu, Sci. Rep. **6**, 37774 (2016).
[24] P. C. Li, Y. L. Sheu, C. Laughlin, and S. I. Chu, Nat. Commun. **6**, 7178 (2015).
[25] M. Chini *et al.*, Nat. Photonics **8**, 437 (2014).
[26] H. Soifer, P. Botheron, D. Shafir, A. Diner, O. Raz, B. D. Bruner, Y. Mairesse, B. Pons, and N. Dudovich, Phys. Rev. Lett. **105**, 143904 (2010).
[27] X. M. Tong and S. I. Chu, Chem. Phys. **217**, 119 (1997).
[28] X. Chu and S. I. Chu, Cecil Laughlin, Phys. Rev. A **64**, 013406 (2001).
[29] Y. C. Chen, M. Y. Cheng, and H. T. Wu, J. R. Statist. Soc. B **76**, 651 (2014).
[30] H. T. Wu, Y. H. Chan, Y. T. Lin, and Y. H. Yeh, Appl. Comput. Harmon. Anal. **36**, 354 (2014).
[31] Y. L. Sheu, L. Y. Hsu, H. T. Wu, P. C. Li, and S. I. Chu, AIP Adv. **4**, 117138 (2014).
[32] X. Chu and S. I. Chu, Phys. Rev. A **63**, 013414 (2000).
[33] D. A. Telnov and S. I. Chu, Phys. Rev. A **76**, 043412 (2007).
[34] P. C. Li, Cecil Laughlin, and S. I. Chu, Phys. Rev. A **89**, 023431 (2014).
[35] P. C. Li, Y. L. Sheu, and S. I. Chu, Phys. Rev. A **101**, 011401(R) (2020).